JAERI-M
9456

ELECTROSTATIC BALLOONING MODE

April 1981

Takashi TUDA, Kimitaka ITOH,
Shinji TOKUDA and Sanae-Inoue ITOH*

日本原子力研究所
Japan Atomic Energy Research Institute

JAERI-M 9456

Electrostatic Ballooning Mode

Takashi TUDA, Kimitaka ITOH, Shinji TOKUDA and Sanae-Inoue ITOH*

Division of Thermonuclear Fusion Research,

Tokai Research Establishment, JAERI

(Received March 25, 1981)

Numerical solution of high-n electrostatic ballooning mode is obtained without approximations. We keep correct forms of electron and ion responses to the wave. We find instabilities which arise due to toroidal effects. The dependences on the aspect ratio, magnetic shear, and wave length are also studied. The growth rate γ is large and satisfies the relation $\omega<\gamma\sim\omega_*$. Depending on the parameters the real frequency ω changes its sign. The drift mode, which has been found stable in a slab plasma, persists in the toroidal plasma remaining almost always stable.

The density fluctuations in tokamaks, which have been observed by use of the microwave scattering method, can be qualitatively explained by the theory of the electrostatic ballooning mode.

Keywords: Ballooning mode, Toroidal Plasma, Drift instability, Matrix method Difference-Differential Equaiton, Numerical Solution, Tokamak

---

*) Institute for Fusion Theory, Hiroshima University

JAERI-M 9456

静電的バルーニング・モード

日本原子力研究所東海研究所核融合研究部
津田　孝・伊藤公孝・徳田伸二・伊藤早苗*

（1981年3月25日受理）

高モード数の静電的なバルーニング・モードを近似を用いずに数値的に解いた。イオンおよび電子の波に対する応答は正確に取り入れた。トロイダル効果によって顕現するいくつかの不安定性を見つけることができ，それらのアスペクト比，シェア，波長等に対する依存性を調べた。この不安定性の成長率はドリフト周波数程度で大きく，固有周波数の実部は成長率より小さく，パラメーターによりその符号を変える。スラブ模型での解析では安定であった通常のドリフト波は，トロイダル効果を取り入れても，はとんどのパラメーター領域で安定にとどまる。

トカマク装置における散乱測定で観測されているプラズマ密度の揺動はこの静電的バルーニング・モードによって定性的に説明が可能である。

＊　広島大学核融合理論研究センター

Contents

目　　次

1. Introduction

Much work has been done for drift wave ballooning mode in toroidal devices[1-11]. We still have not yet obtained the comprehensive theory of drift wave to explain experimental results[12,13]. The drift-like fluctuations have been observed, whose frequency range spreads from zero to ω_* (drift frequency) for fixed perpendicular wavenumber $k_\perp$, while the spectrum in the wave number space is also broad for the fixed real frequency. In order to explain these results, many extensive analyses, linear and nonlinear, of drift waves have been made. However, these efforts up to today seem to be unsuccessful.

In actual plasmas, the toroidal effects to the stability, i.e., couplings between the Fourier modes which have adjacent poloidal mode numbers, are inevitable. To include the correct toroidal effects there have been theoretical developments. Toroidal modes have been solved by use of weak coupling or strong coupling approximations[2,3,6,7]. Also was made the analysis using the Fourier decomposing ballooning representation[14], and the numerical calculations were performed to get two dimensional structures[4,9]. The weak and strong coupling approximations limit the available parameter regions of the analyses. Combining the perturbation techniques with the ballooning representations, toroidicity induced modes other than the usual drift wave have been found for particular parameters[8,10]. The application of the ballooning representation found difficulty in including the correct form of electron non-adiabatic responses. The drift wave theory in a slab in sheared magnetic field has clarified that the wave is stable and the electron response is important to dictate the stability[15,16]. Therefore to study the stability of toroidal modes in connection with the results obtained in the slab, we have to include the full electron response.

In this paper we solve the difference-differential equation of the electrostatic ballooning mode. We retain the mode coupling effect and the full electron response in a correct form. To avoid the ambiguities of limiting approximations, we directly solve the equation by use of a newly developed numerical method. This is a combination method of the matrix formalism and the Newton's method.

We numerically found many branches in toroidal plasmas. We here discuss three typical branches. Their relations to the slab branches are

clarified. One of three (A) is a usual drift wave of $\omega \simeq \omega_*$, which is stable in a slab in sheared magnetic field[14,15], remains to be a damped mode even for the case of the finite value of ε ($\varepsilon = r/R$; r and R are minor and major radii). This result agrees with the one analysed in Refs.[6,7,10]. The next branch (B) is newly induced by the toroidal coupling and is always unstable. The last branch (C) is a highly damped mode in the slab while rapidly becomes most unstable when we turn on the toroidality ε. The modes which belong to the latter two branches have real frequencies around $\omega \simeq 0$ and have large growth rates, $\gamma \gtrsim |\omega|$[17].

Mode identification for the numerical results are also made by use of the variational principle method[18].

Existence of these three branches has been first reported in Ref.[19]. We here extend it to study the parameter dependences of these modes and show that the existence of the electrostatic ballooning instability is "universal" in toroidal plasmas.

Throughout the paper, we entirely neglect the trapped particle effects for simplicity. We treat the electrostatic modes in low-β (β : plasma pressure / magnetic pressure) plasmas.

2. Basic Equations

The coordinates are taken as (r, θ, φ) (θ, φ are poloidal and toroidal angles). We employ the tokamak ordering, $B_\theta^2/B_\varphi^2 \ll 1$, and assume that the magnetic surfaces are circular and concentric to allow the theoretical investigations. Choosing the equilibrium distribution function as

$$f_0 = \frac{n_0}{(2\pi)^{3/2} v_T^3} \exp[-(r-mv_\varphi/eB_\theta)/L_n - v^2/2v_T^2], \qquad (1)$$

we calculate the electron and ion density fluctuations including the toroidal and curvature drift of particles. The perturbed electrostatic potential is presented in the form as

$$\hat{\phi}(\vec{r},t) = \sum \phi_m(r) \exp(-i\omega t + im\theta - in\varphi) \quad .$$

Assuming that the r variation of the mode is weak, $\rho_i^2 d^2/dr^2 \ll 1$, the basic

clarified. One of three (A) is a usual drift wave of $\omega \simeq \omega_*$, which is stable in a slab in sheared magnetic field[14,15], remains to be a damped mode even for the case of the finite value of ε ($\varepsilon = r/R$; r and R are minor and major radii). This result agrees with the one analysed in Refs.[6,7,10]. The next branch (B) is newly induced by the toroidal coupling and is always unstable. The last branch (C) is a highly damped mode in the slab while rapidly becomes most unstable when we turn on the toroidality ε. The modes which belong to the latter two branches have real frequencies around $\omega \simeq 0$ and have large growth rates, $\gamma \gtrsim |\omega|$[17].

Mode identification for the numerical results are also made by use of the variational principle method[18].

Existence of these three branches has been first reported in Ref.[19]. We here extend it to study the parameter dependences of these modes and show that the existence of the electrostatic ballooning instability is "universal" in toroidal plasmas.

Throughout the paper, we entirely neglect the trapped particle effects for simplicity. We treat the electrostatic modes in low-β (β : plasma pressure / magnetic pressure) plasmas.

2. Basic Equations

The coordinates are taken as (r, θ, φ) (θ, φ are poloidal and toroidal angles). We employ the tokamak ordering, $B_\theta^2/B_\varphi^2 \ll 1$, and assume that the magnetic surfaces are circular and concentric to allow the theoretical investigations. Choosing the equilibrium distribution function as

$$f_0 = \frac{n_0}{(2\pi)^{3/2} v_T^3} \exp[-(r - mv_\varphi/eB_\theta)/L_n - v^2/2v_T^2], \qquad (1)$$

we calculate the electron and ion density fluctuations including the toroidal and curvature drift of particles. The perturbed electrostatic potential is presented in the form as

$$\hat{\phi}(\vec{r},t) = \sum \phi_m(r) \exp(-i\omega t + im\theta - in\varphi) \quad .$$

Assuming that the r variation of the mode is weak, $\rho_i^2 d^2/dr^2 \ll 1$, the basic

equations have been derived in a set of coupled differential equations as[6]

$$\left[\frac{d^2}{dx^2} - k^2\rho_i^2 + P(x) \right] \phi_m(x)$$

$$= \frac{\varepsilon\omega_*}{\tau\omega} \left\{ \left(1 - \frac{1}{k\rho_i}\frac{d}{dx}\right) \phi_{m-1}(x) + \left(1 + \frac{1}{k\rho_i}\frac{d}{dx}\right) \phi_{m+1}(x) \right\} , \qquad (2)$$

where the following notations are used; $x = (r-r_s)/\rho_i$, $q(r_s) = m/n$, $k = m/r$, $\xi = \omega/\sqrt{2}|k_{//}|v_T$, $k_{//} = (m-nq)/qR$, $\tau = T_e/T_i$, $\omega_* = cT_e k/eBL_n$, $n_0/L_n = |dn_0/dr|$, $P(x) = \{(\omega_*-\omega)Z'(\xi_e)/(\omega\tau+\omega_*) - Z'(\xi_i)\}/2\xi_i Z(\xi_i)$, $\varepsilon = L_n/R$ and other notations are standard. The terms in the right hand side denote the mode coupling due to the toroidal effects.

In considering the high n (i.e., $n \gg 1/\varepsilon$) ballooning mode we see that the equation (2) is invariant for the transformation of $(x,m) \to (x-\Delta, m+1)$, where $\Delta\rho_i$ is the distance between two adjacent mode rational surfaces, $\Delta = 1/k\rho_i s$ ($s = rq'/q$). Noting this fact, the set of coupled differential equations (2) is reduced to a one dimensional difference-differential equation

$$\left[\frac{d^2}{dx^2} - k^2\rho_i^2 + P(x) \right] \phi(x)$$

$$= \frac{\varepsilon\omega_*}{\tau\omega} \left\{ \left(1 - \frac{1}{k\rho_i}\frac{d}{dx}\right)\phi(x+\Delta) + \left(1 + \frac{1}{k\rho_i}\frac{d}{dx}\right)\phi(x-\Delta) \right\} \qquad (3)$$

with

$$\phi_j(x) = \phi(x-j\Delta) \qquad (3')$$

where $j = m - m_0$ and x is redefined as $q(x=0) = m_0/n$.

3. Numerical Calculation

The equation (3) is solved numerically with the aid of the matrix formulation. Introducing mesh width h and writing $x_j = hj$ and $\phi_j = \phi(x_j)$, Eq.(3) is formulated in a set of coupled linear equations as

equations have been derived in a set of coupled differential equations as[6)]

$$\left[\frac{d^2}{dx^2} - k^2\rho_i^2 + P(x) \right] \phi_m(x)$$

$$= \frac{\varepsilon\omega_*}{\tau\omega} \left\{ \left(1 - \frac{1}{k\rho_i}\frac{d}{dx}\right) \phi_{m-1}(x) + \left(1 + \frac{1}{k\rho_i}\frac{d}{dx}\right) \phi_{m+1}(x) \right\} , \qquad (2)$$

where the following notations are used; $x = (r-r_s)/\rho_i$, $q(r_s) = m/n$, $k = m/r$, $\xi = \omega/\sqrt{2}|k_{//}|v_T$, $k_{//} = (m-nq)/qR$, $\tau = T_e/T_i$, $\omega_* = cT_e k/eBL_n$, $n_0/L_n = |dn_0/dr|$, $P(x) = \{(\omega_*-\omega)Z'(\xi_e)/(\omega\tau+\omega_*) - Z'(\xi_i)\}/2\xi_i Z(\xi_i)$, $\varepsilon = L_n/R$ and other notations are standard. The terms in the right hand side denote the mode coupling due to the toroidal effects.

In considering the high n (i.e., $n >> 1/\varepsilon$) ballooning mode we see that the equation (2) is invariant for the transformation of $(x,m) \rightarrow (x-\Delta, m+1)$, where $\Delta\rho_i$ is the distance between two adjacent mode rational surfaces, $\Delta = 1/k\rho_i s$ ($s = rq'/q$). Noting this fact, the set of coupled differential equations (2) is reduced to a one dimensional difference-differential equation

$$\left[\frac{d^2}{dx^2} - k^2\rho_i^2 + P(x) \right] \phi(x)$$

$$= \frac{\varepsilon\omega_*}{\tau\omega} \left\{ \left(1 - \frac{1}{k\rho_i}\frac{d}{dx}\right)\phi(x+\Delta) + \left(1 + \frac{1}{k\rho_i}\frac{d}{dx}\right)\phi(x-\Delta) \right\} \qquad (3)$$

with

$$\phi_j(x) = \phi(x-j\Delta) \qquad (3')$$

where $j = m - m_0$ and x is redefined as $q(x=0) = m_0/n$.

3. Numerical Calculation

The equation (3) is solved numerically with the aid of the matrix formulation. Introducing mesh width h and writing $x_j = hj$ and $\phi_j = \phi(x_j)$, Eq.(3) is formulated in a set of coupled linear equations as

$$
\begin{aligned}
&- \frac{\varepsilon\omega_*}{2\tau\omega}\frac{h}{k\rho_i}\,\phi_{j-n-1} + \frac{\varepsilon\omega_*}{\tau\omega}\,h^2\phi_{j-n} + \frac{\varepsilon\omega_*}{2\tau\omega}\frac{h}{k\rho_i}\,\phi_{j-n+1} \\
&- \phi_{j-1} + \left(2 - P_j h^2 + k^2\rho_i^2 h^2 \right)\phi_j - \phi_{j+1} \qquad (j = -N....N) \\
&+ \frac{\varepsilon\omega_*}{2\tau\omega}\frac{h}{k\rho_i}\,\phi_{j+n-1} + \frac{\varepsilon\omega_*}{\tau\omega}\,h^2\phi_{j+n} - \frac{\varepsilon\omega_*}{2\tau\omega}\frac{h}{k\rho_i}\,\phi_{j+n+1} = 0 , \qquad (4)
\end{aligned}
$$

where $P_j = P(x_j)$ and $n = \Delta/h$. The truncation length is chosen large enough that $\phi(x)$ exponentially damps off at $|x| > hN$. The solution of Eq.(3) conserves the parity, therefore we need to solve $\phi(x)$ only in the domain $0 \leq x \leq hN$, selecting either $\phi(-x) = \phi(x)$ or $\phi(-x) = -\phi(x)$. We here obtain the even mode, i.e., $\phi(-x) = \phi(x)$. Noting this relation, Eq.(4) is rewritten as

$$
\begin{pmatrix} & & \\ & a_{ij} & \\ & & \end{pmatrix}
\begin{pmatrix} \phi_0 \\ \vdots \\ \phi_N \end{pmatrix} = 0 \qquad (5)
$$

where tridiagonal terms arises from d^2/dx^2 and the slab potential $k^2\rho_i^2 + P$, and off-diagonal terms appear for $j = i\pm n$, $i\pm n\pm 1$, $n-i$ and $n-i\pm 1$ due to the toroidal coupling. The equation (5) yields nontrivial solution if and only if

$$
D(\omega) \equiv \det(a_{ij}) = 0 \qquad (6)
$$

holds. $D(\omega)$ depends on ω through $Z(\omega/\sqrt{2}|k_{//}|v_T)$; the equation $D(\omega) =$ is a transcendental equation of ω and is solved by contour method with Newton method in iteration. It is emphasized that the intensive convergence study is performed on the mesh width h and the truncation length hN. The convergence as well as the accuracy is found to be satisfactory. The precise descriptions on the convergence, accuracy and efficiency of our numerical procedure will be given in a forthcomming paper.

The figure 1 shows the eigenvalues in the Reω - Imω plane; the toroidality

ε is varied from 0 to 0.1. Other parameters are $k\rho_i = 0.2$, $s = 1$ and $\tau = 1$. We take $m_i/m_e = 1836$. In varying ε, q also changes so that the shear parameter L_s/L_n is kept constant ($L_s/L_n = q/\varepsilon s$, 32 in this case) to illustrate the relation between toroidal mode and slab mode. We find several unstable and stable branches; among them three of them require attentions and studies. One is the solution which merges to the Pearlstein-Berk solution in the slab limit (Branch A). This is denoted by the dotted and dashed line. It remains stable even if toroidal mode coupling is introduced. This confirms the theoretical analyses in Refs.[6,10], but contradicts to the numerical result of Ref.[8]. The instability is realized for modes which have small real frequency. The dashed line (branch B) shows one of the ballooning modes. The eigen value ω goes to 0 as ε approaches to zero; the higher modes of this branch (which have more nodes in radial direction and smaller growth rates) are also found as is predicted in §4. It is noted that there is no criterion of ε for the existence of the ballooning modes. Addition of infinitesimal toroidality leads an onset of instabilities. The surprizing is that the most unstable mode for $\varepsilon = 0.1$ is connected to a slab mode which is determined by the electron response and is highly damped (so that has not been studied well in the slab theory). This is shown by the solid line, branch C. This fact clarifies the importance to correctly evaluate the electron response near the mode rational surface.

The radial mode structures $\phi(x)$ of these three branches are shown for the parameters $k\rho_i = 0.2$, $s = 1$, $q = 3.2$, $\varepsilon = 0.1$ ($L_s/L_n = 32$ and $\Delta = 5$). The figure 2a is for the most unstable mode C (the solid line in Fig.1), Fig.2b for the 2nd branch B (dashed line in Fig.1), and Fig.2c for the branch A. The two dimensional structure $\Phi(x,\theta)$ is readily obtained by

$$\Phi(x,\theta) = \sum_m \phi(x-m\Delta)\exp(im\theta)$$

as shown in Fig.2d. The radial mode structure ϕ is localized to the region $|x| \lesssim \Delta$ for Fig.2a, the poloidal structure of Φ shows the poloidal ballooning with the width approximately $1/\Delta$.

The parameter dependences of the eigenvalues of these three branches are studied. The dependences on ε is shown in Fig.3 (in this case q is

kept constant), $k\rho_i$ varies in Fig.4 and s varies in Fig.5, while other parameters are fixed ($\varepsilon = 0.1$, $s = 1$, $q = 3.2$, $k\rho_i = 0.2$ and $\tau = 1$). The solid line, dashed line and the dotted and dashed line correspond to those in Fig.1 respectively.

The most important issues of these results are that i) electrostatic ballooning modes are almost always unstable in the presence of the toroidality, ii) the growth rate γ easily exceeds the real frequency ω and the real part of the eigenvalue is small compared to ω_* ($\omega/\omega_* \sim O(\varepsilon)$ typically holds for $\varepsilon \ll 1$) iii) the radial structure of the electron response is essential for the instability and that iv) the drift modes in the slab geometry persists in toroidal geometry but remains stable or becomes weakly unstable at most. It should be noted that, for unstable ballooning modes, the real frequency locates from $-0.1\omega_*$ to $0.3\ \omega_*$ as $k\rho_i$ changes 0.5 to 0.1. Modes with wide range of k becomes unstable satisfying $\omega < \gamma \sim \omega_*$; in typical parameters of toroidal experiments, real frequencies of unstable modes are not close to ω_* (or $\omega_*(1-k^2\rho_i^2\tau)$) and do not show the strong tendency to propagate in the electron diamagnetic drift direction. Our calculation should be compared to experimental results where the fluctuation spectrum has a peak around not $\omega \simeq \omega_*$ but $\omega \simeq 0$. Our analysis suggests that the fluctuations are due to these ballooning instabilities.

Finally T_e/T_i dependence is illustrated in Fig.6. As is discussed in §4, the shear term dominates the dispersion of the ballooning modes when τ becomes large as $1/\varepsilon$; the ballooning instability branches go to zero as τ approaches to $1/\varepsilon$ ($\varepsilon = 0.1$ in Fig.6). This may be one of the reasons that the ballooning modes found in this paper were not obtained in Refs.[8,10].

4. Mode Identifications by use of Variational Principle

To understand the exact solutions of Eq.(3), let us discuss the mode identification and the stability analysis using the variational principle method.

Operating $\int \phi\, dx$ to Eq.(3), the quadratic form with respect to ϕ, L, is given by

kept constant), $k\rho_i$ varies in Fig.4 and s varies in Fig.5, while other parameters are fixed ($\varepsilon = 0.1$, $s = 1$, $q = 3.2$, $k\rho_i = 0.2$ and $\tau = 1$). The solid line, dashed line and the dotted and dashed line correspond to those in Fig.1 respectively.

The most important issues of these results are that i) electrostatic ballooning modes are almost always unstable in the presence of the toroidality, ii) the growth rate γ easily exceeds the real frequency ω and the real part of the eigenvalue is small compared to ω_* ($\omega/\omega_* \sim O(\varepsilon)$ typically holds for $\varepsilon \ll 1$) iii) the radial structure of the electron response is essential for the instability and that iv) the drift modes in the slab geometry persists in toroidal geometry but remains stable or becomes weakly unstable at most. It should be noted that, for unstable ballooning modes, the real frequency locates from $-0.1\omega_*$ to $0.3\ \omega_*$ as $k\rho_i$ changes 0.5 to 0.1. Modes with wide range of k becomes unstable satisfying $\omega < \gamma \sim \omega_*$; in typical parameters of toroidal experiments, real frequencies of unstable modes are not close to ω_* (or $\omega_*(1-k^2\rho_i^2\tau)$) and do not show the strong tendency to propagate in the electron diamagnetic drift direction. Our calculation should be compared to experimental results where the fluctuation spectrum has a peak around not $\omega \simeq \omega_*$ but $\omega \simeq 0$. Our analysis suggests that the fluctuations are due to these ballooning instabilities.

Finally T_e/T_i dependence is illustrated in Fig.6. As is discussed in §4, the shear term dominates the dispersion of the ballooning modes when τ becomes large as $1/\varepsilon$; the ballooning instability branches go to zero as τ approaches to $1/\varepsilon$ ($\varepsilon = 0.1$ in Fig.6). This may be one of the reasons that the ballooning modes found in this paper were not obtained in Refs.[8,10].

4. Mode Identifications by use of Variational Principle

To understand the exact solutions of Eq.(3), let us discuss the mode identification and the stability analysis using the variational principle method.

Operating $\int \phi\, dx$ to Eq.(3), the quadratic form with respect to ϕ, L, is given by

$$L = \int dx\,\phi\,[\,\phi'' - k^2\rho_i^2\phi + P(x)\phi - \frac{\varepsilon\omega_*}{\tau\omega}\{(1-\frac{1}{k\rho_i}\frac{d}{dx})\phi(x+\Delta) + (1+\frac{1}{k\rho_i}\frac{d}{dx})\phi(x-\Delta)\}\,]. \tag{7}$$

Its variational δL should be zero with the constraint $L = 0$. We use the trial function to be

$$\phi(x) = \exp(-\alpha x^2/2) \tag{8}$$

for we are interested in localized mode, and obtain the equations for (α,ω) as

$$L = \frac{\omega_* - \omega}{\omega\tau+\omega_*} - k^2\rho_i^2 + \frac{(1+\tau)\omega_*}{\tau(\omega\tau+\omega_*)\omega}\frac{L_n^2}{L_s^2}\frac{1}{2\alpha} - \frac{\alpha}{2} - \frac{\omega_* - \omega}{\omega\tau+\omega_*}\sqrt{2}\,i\nu\left(\ell n\frac{\sqrt{2}}{\nu} - C + \frac{i\pi}{4} - 4\nu\right) - \frac{2\varepsilon\omega_*}{\tau\omega}(1+s\Delta^2\alpha)e^{-\frac{\alpha}{4}\Delta^2} = 0 \tag{9}$$

and

$$\frac{\partial L}{\partial\alpha} = 0 \tag{10}$$

($\nu \equiv \sqrt{\alpha}x_e$, $\sqrt{2}k_{//}(x_e)v_e = \omega_*$ and $\nu \ll 1$). Solving Eqs.(9) and (10) with respect to α, two typical modes are found keeping the analytical insight.

The branch A is discussed in Ref.[18] and is understood that it is generated by the balance of slab terms. As ω is of the order of ω_*, the mode is less affected by the toroidal coupling.

Another important branch is generated by the toroidal effects; for small ω mode such that $\omega/\omega_* \sim O(\varepsilon)$, the toroidal term gives a contribution of the same magnitude as the slab terms. To investigate such mode we introduce the ordering $\omega/\omega_* \sim O(\varepsilon)$ to have

$$1 - k^2\rho_i^2 - (1+\tau)\omega/\omega_* + \frac{(1+\tau)\omega_*}{\tau\,\omega}\frac{L_n^2}{L_s^2}\frac{1}{2\alpha} - \frac{\alpha}{2} - \sqrt{2}\,i\nu\{\ell n\frac{\sqrt{2}}{\nu} - C + \frac{i\pi}{4} - 4\nu\} - \frac{2\varepsilon\omega_*}{\tau\omega}(1+s\Delta^2\alpha)\,e^{-\frac{\alpha}{4}\Delta^2} = 0 \tag{11}$$

unless $\tau > 1/\varepsilon$. First we temporaly neglect ν and Eq.(10) is reduced to

$$-\frac{\omega}{2\omega_*} - \frac{(1+\tau)}{2}\frac{L_n^2}{\tau L_s^2}\frac{1}{\alpha^2} - \frac{2\varepsilon}{\tau}\left\{s\Delta^2 - \frac{\Delta^2}{4}(1+s\Delta^2\alpha)\right\} e^{-\frac{\alpha}{4}\Delta^2} = 0 \quad . \tag{12}$$

In the limit $L_n^2/L_s^2 < \varepsilon \to 0$, we have

$$\frac{\omega}{\omega_*} \simeq \frac{4(1+s\Delta^2\alpha)}{|2-\alpha|}\exp(-\alpha\Delta^2/4)\,\frac{\varepsilon}{\tau} \tag{13}$$

and

$$\alpha \simeq 4/\Delta^2 \tag{14}$$

(this is a simplified notation in $s\Delta^2 > 1$). This branch can become unstable due to the electron Landau resonance (ν term in Eq.(11)) as

$$\frac{\gamma}{\omega} \simeq \frac{2\sqrt{2}}{|2-\alpha|}\,\nu\,\ell n\,\frac{\sqrt{2}}{\nu} \tag{15}$$

This mode is identified as the branch B. If we employ test functions as $H_n(\sqrt{\alpha}x)\exp(-\alpha x^2/2)$ ($n > 0$ and H_n is an Hermite polinomial), the higher mode of this branch can be obtained. We here note that the extremely large value of τ changes the solution. If $\tau > 1/\varepsilon$ holds, then ω_*^2/ω^2term arises from the ion convection term ($\propto L_n^2/L_s^2$) in Eq.(11). This breaks the ordering $\omega/\omega_* \sim \varepsilon$ but leads $\omega/\omega_* \sim \varepsilon^0$. The equarion (13) also shows that, if we directly extraporate Eq.(13) into the region $\tau > 1/\varepsilon$, $\omega/\omega_* \sim \varepsilon/\tau \lesssim O(\varepsilon^2)$. Therefore the electrostatic ballooning mode may exist in the parameter region $\tau < 1/\varepsilon$, which is satisfied in the present and future experiments and has been almost always satisfied in previous experiments.

5. Conclusions and Discussions

In conclusion we have investigated the electrostatic high-n ballooning mode in toroidal geometry. We directly solve the governing equation which includes the mode couplings and full electron and ion responses. We did not use any approximation in solving Eq.(3). We develop a new numerical method

unless $\tau > 1/\varepsilon$. First we temporaly neglect ν and Eq.(10) is reduced to

$$-\frac{\omega}{2\omega_*} - \frac{(1+\tau)}{2}\frac{L_n^2}{\tau L_s^2}\frac{1}{\alpha^2} - \frac{2\varepsilon}{\tau}\{s\Delta^2 - \frac{\Delta^2}{4}(1+s\Delta^2\alpha)\}\, e^{-\frac{\alpha}{4}\Delta^2} = 0 \quad . \tag{12}$$

In the limit $L_n^2/L_s^2 < \varepsilon \to 0$, we have

$$\frac{\omega}{\omega_*} \simeq \frac{4(1+s\Delta^2\alpha)}{|2-\alpha|}\exp(-\alpha\Delta^2/4)\,\frac{\varepsilon}{\tau} \tag{13}$$

and

$$\alpha \simeq 4/\Delta^2 \tag{14}$$

(this is a simplified notation in $s\Delta^2 > 1$). This branch can become unstable due to the electron Landau resonance (ν term in Eq.(11)) as

$$\frac{\gamma}{\omega} \simeq \frac{2\sqrt{2}}{|2-\alpha|}\,\nu\,\ell n\,\frac{\sqrt{2}}{\nu} \tag{15}$$

This mode is identified as the branch B. If we employ test functions as $H_n(\sqrt{\alpha}x)\exp(-\alpha x^2/2)$ ($n > 0$ and H_n is an Hermite polinomial), the higher mode of this branch can be obtained. We here note that the extremely large value of τ changes the solution. If $\tau > 1/\varepsilon$ holds, then ω_*^2/ω^2term arises from the ion convection term ($\propto L_n^2/L_s^2$) in Eq.(11). This breaks the ordering $\omega/\omega_* \sim \varepsilon$ but leads $\omega/\omega_* \sim \varepsilon^0$. The equarion (13) also shows that, if we directly extraporate Eq.(13) into the region $\tau > 1/\varepsilon$, $\omega/\omega_* \sim \varepsilon/\tau \lesssim O(\varepsilon^2)$. Therefore the electrostatic ballooning mode may exist in the parameter region $\tau < 1/\varepsilon$, which is satisfied in the present and future experiments and has been almost always satisfied in previous experiments.

5. Conclusions and Discussions

In conclusion we have investigated the electrostatic high-n ballooning mode in toroidal geometry. We directly solve the governing equation which includes the mode couplings and full electron and ion responses. We did not use any approximation in solving Eq.(3). We develop a new numerical method

where we used both the matrix formula technique and the Newton's method to find out the eigenmode structures.

We identified three typical modes. One is stable drift branch whose frequency is about ω_* and is corresponding to the stable drift wave in the slab. This branch remains weak instability even in the toroidal geometry. The next is the mode which is highly damped mode in the slab geometry. This mode has the real frequency much less than ω_* and does become most unstable in toroidal geometry. For the case of $\varepsilon = 0.1$, its growth rate γ is much greater than the real frequency, $|\omega| < \gamma$. The third one does not exist in slab geometry. However, if we put the toroidal coupling, this mode arises from the $\omega = \gamma = 0$ point. Its real frequency is near $\omega \sim 0$ and $|\omega| < \gamma$.

In addition to it, we also identified them by use of the variational principle.

When one uses various approximations to solve Eq.(3), one may miss-interprete the relations between the slab mode and toroidal mode. We also found the toroidality induced mode is always unstable.

Throughout the paper we neglected the trapped particle effects and set the scope to the toroidal effects on the modes. Also neglected are the magnetic well effect and the modification of the plasma crosssection. Our calculation can be easily applied to the study of these effects. The electron temperature gradient effect is also studied and found to have a weak effect on the stability of the electrostatic ballooning mode. The effect of toroidal drift of electrons is fairly small, is order of v_i/v_e, hence is neglected.

For the finite but small β plasma we have to consider the coupling between Alfvén branch and drift branch. These analysis by use of the same numerical technique will be presented in a separate paper[20]. Also should be done is the analyses of low m kinetic helical instabilities[21] to study the disruption protect in high temperature plasmas.

The authors wish to thank the members of the theory group of JAERI for usefull helps and discussions. Thanks are also due to Drs. T.Takeda, M. Tanaka and Y.Obata for continuous encouragements. One of the authors (S.I. I.) shows sincere gratitudes to Dr. Y.Obata for hospitalities.

where we used both the matrix formula technique and the Newton's method to find out the eigenmode structures.

We identified three typical modes. One is stable drift branch whose frequency is about ω_* and is corresponding to the stable drift wave in the slab. This branch remains weak instability even in the toroidal geometry. The next is the mode which is highly damped mode in the slab geometry. This mode has the real frequency much less than ω_* and does become most unstable in toroidal geometry. For the case of $\varepsilon = 0.1$, its growth rate γ is much greater than the real frequency, $|\omega| < \gamma$. The third one does not exist in slab geometry. However, if we put the toroidal coupling, this mode arises from the $\omega = \gamma = 0$ point. Its real frequency is near $\omega \sim 0$ and $|\omega| < \gamma$.

In addition to it, we also identified them by use of the variational principle.

When one uses various approximations to solve Eq.(3), one may miss-interprete the relations between the slab mode and toroidal mode. We also found the toroidality induced mode is always unstable.

Throughout the paper we neglected the trapped particle effects and set the scope to the toroidal effects on the modes. Also neglected are the magnetic well effect and the modification of the plasma crosssection. Our calculation can be easily applied to the study of these effects. The electron temperature gradient effect is also studied and found to have a weak effect on the stability of the electrostatic ballooning mode. The effect of toroidal drift of electrons is fairly small, is order of v_i/v_e, hence is neglected.

For the finite but small β plasma we have to consider the coupling between Alfvén branch and drift branch. These analysis by use of the same numerical technique will be presented in a separate paper[20]. Also should be done is the analyses of low m kinetic helical instabilities[21] to study the disruption protect in high temperature plasmas.

The authors wish to thank the members of the theory group of JAERI for usefull helps and discussions. Thanks are also due to Drs. T.Takeda, M. Tanaka and Y.Obata for continuous encouragements. One of the authors (S.I. I.) shows sincere gratitudes to Dr. Y.Obata for hospitalities.

References

1] J.B.Taylor, Plasma Physics and Controlled Nuclear Fusion Research, (IAEA, Vienna, 1977) Vol.2,p323.

2] W.M.Tang, Nucl. Fusion 18 (1978) 1089.

3] W.Horton Jr., R.Estes, H.Kwak and Duk-In Choi, Phys. Fluids 21 (1978) 1366.

4] G.Rewoldt, W.M.Tang and E.A.Frieman, Phys. Fluids 21 (1978) 1513.

5] R.J.Hastie, K.W.Hesketh and J.B.Taylor, Nucl. Fusion 19 (1979) 1223.

6] K.Itoh, T.Tuda and S.Inoue, J. Phys. Soc. Japan 48 (1980) 258.

7] S.Inoue, K.Itoh and S.Yoshikawa, J. Phys. Soc.Japan 49 (1980) 367.

8] K.W.Hesketh, Nucl. Fusion 20 (1980) 1013.

9] E.A.Frieman, G.Rewoldt, W.M.Tang and A.H.Glasser, Phys. Fluids 23 (1980) 1750.

10] C.Z.Cheng and Liu Chen, Phys. Fluids 23 (1980) 1770.

11] W.M.Tang, J.W.Connor and R.J.Hastie, Nucl. Fusion 20 (1980) 1439.

12] C.M.Surko and R.E.Slusher, Phys. Rev. Lett. 37 (1976) 1747.

13] R.J.Goldston, E.Mazzucato, R.E.Slusher and C.M.Surko, Plasma Physics and Controlled Nuclear Fusion Research (IAEA, Vienna, 1977) Vol.1,p371.

14] J.W.Connor, R.J.Hastie and J.B.Taylor, Proc. R. Soc. A365 (1979) 1.

15] D.W.Ross and S.M.Mahajan, Phys. Rev. Lett. 40 (1978) 324.

16] K.T.Tsang, P.J.Catto, J.C.Whitson and J.Smith, Phys. Rev. Lett. 40 (1978) 327.

17] The instabilities found in Refs.[8,10] seem to belong to these branches. However, the approximations they have used seem to be unsatisfactory to distinguish between B and C branches.

18] T.Tuda, K.Itoh and S.I.Itoh, JAERI-M 9234 (1980, in Japanese).

19] T.Tuda, K.Itoh, S.Tokuda and S.I.Itoh, submitted to Nucl. Fusion.

20] T.Tuda, K.Itoh, S.Tokuda and S.I.Itoh, Sherwood Meeting (1981, Austin). Also submitted to Phys. Rev. Lett.

21] S.I.Itoh and K.Itoh, Nucl. Fusion 21 (1981) 3.

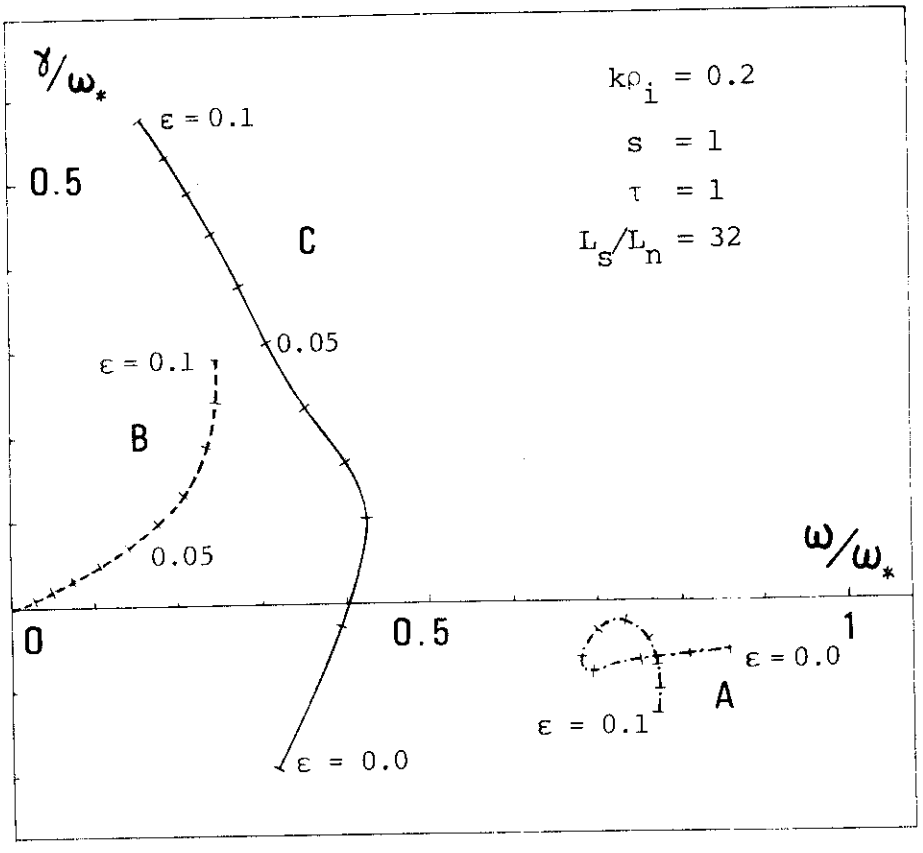

Fig.1 Eigenvalue trajectories of three typical modes (A,B,C) in the Reω - Imω plane. The value of ε varies from 0 to 0.1, which is noted on lines. $k\rho_i$ = 0.2, s = 1, τ= 1 and L_s/L_n = 32.

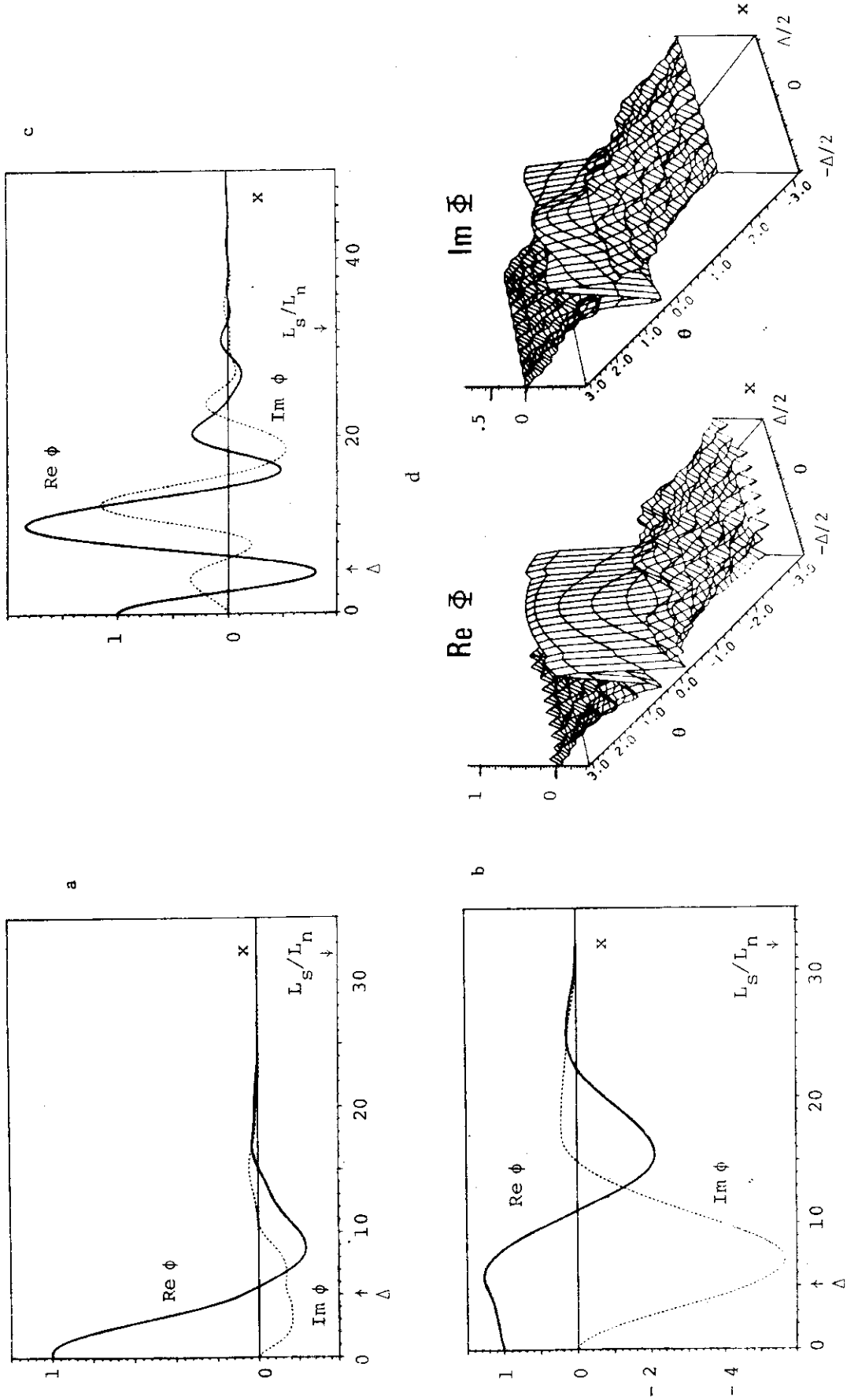

Fig.2 The radial mode structures $\phi(x)$, for the parameters of Fig.1 with $\varepsilon = 0.1$, are shown for C (solid line in Fig.1), B and A cases in Fig.2 a,b,c respectively. The figure 2d shows the 2D mode structure $\Phi(x,\theta)\exp(isx)$ for the parameter of Fig.2a. Φ in the region $-\Delta/2 < x < \Delta/2$ and $-\pi < \theta < \pi$ is shown. $\theta = 0$ corresponds to the outside of the torus.

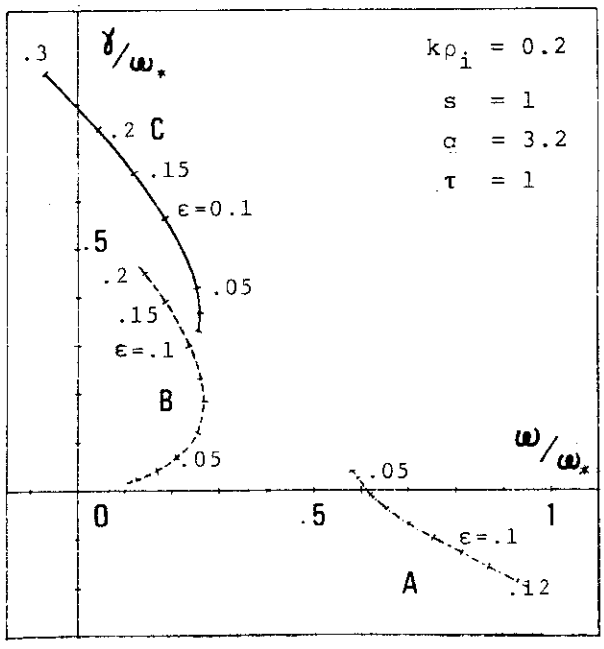

Fig.3 The ε dependences of the eigen values for A,B and C branches for fixed values of q = 3.2, s = 1, τ = 1 and $k\rho_i$ = 0.2.

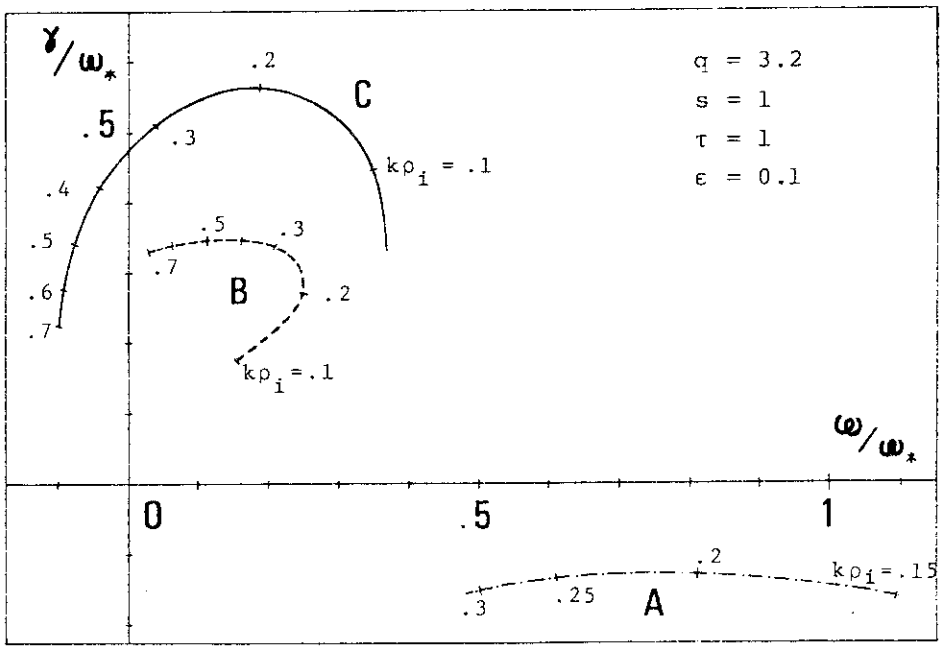

Fig.4 The $k\rho_i$ dependences are shown for ε = 0.1, q = 3.2, s = 1 and τ = 1. We see that the real frequency crosses the ω = 0 line.

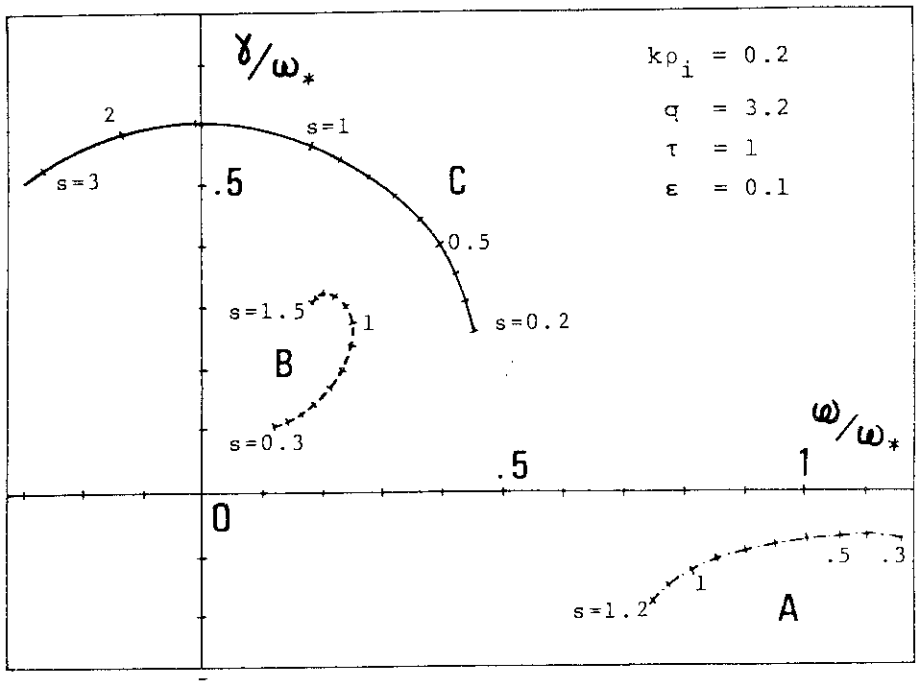

Fig.5 The s dependence. The other parameters are the same as in Fig.2. This figure should be compared with the results in Ref.[8].

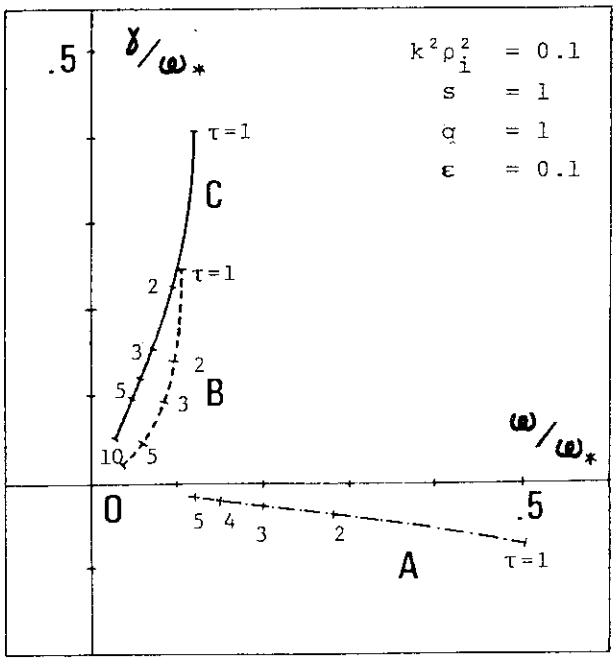

Fig.6 The eigenvalue dependence on T_e/T_i. The parameters are chosen as $k\rho_i = \sqrt{.1}$, $\varepsilon = 0.1$, $s = 1$, and $q = 1$.